OPTO-ELECTRONICS REVIEW **12**(4), 417–428

Generation-recombination effects in high temperature HgCdTe heterostructure photodiodes

A. JÓ WIKOWSKA[1], K. JÓ WIKOWSKI[*2], J. RUTKOWSKI[2], Z. ORMAN[3], and A. ROGALSKI[2]

[1]Warsaw Agricultural University, 166 Nowoursynowska Str., 02-787 Warsaw, Poland
[2]Institute of Applied Physics, Military University of Technology, 2 Kaliskiego Str., 00-908 Warsaw, Poland
[3]Vigo System S.A., 3 Świetlików Str., 01-389 Warsaw, Poland

The effect of built-in electric fields and misfit dislocations on dark currents in high temperature MOCVD HgCdTe infrared heterostructure photodiodes has been investigated. From experimental data results that the current-voltage characteristics at 240 K and 300 K indicate significant contributions from tunnelling effects, which dominate the leakage current mechanism for reverse bias greater than a few tens of milivolts. Standard theoretical models show that Auger generation-recombination processes determine dark current in high temperature HgCdTe photodiodes. But taking into account only Auger mechanisms much overestimated theoretical results are obtained. To explain this fact, a two-dimensional model has been developed to investigate the dark current mechanisms in the vicinity of the junction termination at built-in electric fields. Calculated profiles of the energy bands and electric field along different cross-sections of the photodiode indicate that the electric field achieves a maximum value of the order of mid 10^5 V/cm in the area the junction termination at the HgCdTe heterointerface. In these regions the high density of misfit dislocations are observed too. The presence of high electric field in this area decreases the ionisation energies of trap levels located in region of dislocations core, and hence increases the efficiency of Shockley-Read-Hall generation-recombination process. In addition to diffusion, generation-recombination and trap assisted tunnelling mechanisms, our model include the Poole-Frankel and phonon-trap assisted tunnelling effects in calculations of dynamic resistance of the junctions. The best fit of experimental data with theoretical predictions for dynamic resistance versus temperature has been obtained for dislocation density in the bulk of HgCdTe layer equal to 5×10^{-7} cm^{-2}.

Keywords: HgCdTe photodiodes, generation-recombination effects, Poole-Frankel effect, R_0A product.

1. Introduction

Development of epitaxial technique for the growth of HgCdTe ternary alloys has made possible fabrication of new complex heterostructure device designs [1]. The ability to grow of multilayer heterostructures and layers with compositional gradients and precise doping control allow device fabrications that exploit nonequilibrium phenomena for improvement in infrared detector sensitivity and/or operating temperature. However, in the case of HgCdTe photodiodes, one of the main technical issues is obtaining devices characterized by the dynamic resistance R_d close to theoretically predicted one. Traditional theoretical analysis gives R_d values that may be the orders of magnitude higher than experimentally observed resistances. One reason for this discrepancy is the existence of structural imperfections in epilayers such as dislocations, which can seriously limit device performance. Dislocations strongly affect the electrical properties of semiconductor layers, particularly carrier mobility and lifetime [2,3]. While the strong built-in electrical fields present in heterostructures can give rise to much stronger photovoltaic effects than those observed in homojunction based devices, however, the field induced reduction of trap activation energies can increase thermal generation and create conditions for tunnelling currents.

As it is shown in several articles [4–10], the dynamic resistance of HgCdTe photodiodes at low temperatures is degraded by generation-recombination processes through Shockley-Read-Hall (SRH) trapping centres, with an energy level positioned in the mid-gap region, and most probably associated with mercury vacancies. Additionally, the regions with high dislocation density contain high concentration of trapping centres.

Hitherto it was assumed that in the case of HgCdTe devices operated at the temperatures above 200 K, the influence of point defects and dislocations on generation-recombination process has been insignificant due to serious effect of Auger process [11]. This opinion seems to be right provided that these defects are out of internal regions with built-in electric fields. First of all, strong built-in electric fields occur in the regions with nonuniform distribution of *x*-mole composition and impurities, and near

*e-mail: kjozwikowski@wat.edu.pl

semiconductor surface. If in these regions SRH centres occur, the electrical field activates generation-recombination processes connected with traps. Reasons of that are three well-known mechanisms:

- so-called Frenkl-Pool effect, where the electric field decreases the effective ionization energy of a trap level,
- trap assistant tunnelling (TAT); tunnelling is possible by means of indirect transitions in which impurities or defects within the space-charge region act as intermediate states,
- phonon trap assistant tunnelling (PTAT) with additional contribution of phonons.

These three mechanisms increase emission coefficient and rate of thermal generation-recombination processes. As a result, the space-charge region of p-n junctions generates most of all carriers.

In VIGO/WAT MOCVD Laboratory HgCdTe heterostructures are deposited on GaAs/CdTe composite substrates. The devices fabricated using metalorganic chemical vapour deposition (MOCVD) have dislocation density typically above 10^7 cm^{-2}. The $I(V)$ characteristics of 3–5.5-μm photodiodes indicate on considerable contribution of tunnelling current. It is predicted that generation-recombination processes in dislocation regions enhance contribution of tunnelling current. From this prediction follows necessity of elaboration a new model regarding dislocation generation-recombination effects. This is the aim of this paper. Theoretical predictions of the model are compared with experimental data – dynamic resistance versus bias voltage and temperature.

2. Method of analysis

The analysis of photoelectric effects in semiconductor structures requires solution of a set of transport equations that are comprised of the continuity equations for electrons and holes, Poisson's equation, and the thermal conductivity equation. The transport equations are given by [12,13]

$$\frac{\partial p}{\partial t} = -\frac{1}{q}\nabla\vec{j}_p + G - R, \tag{1}$$

$$\frac{\partial n}{\partial t} = \frac{1}{q}\nabla\vec{j}_n + G - R, \tag{2}$$

$$\nabla^2\Psi = -\frac{q}{\varepsilon\varepsilon_0}\left[N_d^+ - N_a^- + p - n\right] - \frac{1}{\varepsilon}\nabla\Psi\,\nabla\varepsilon, \tag{3}$$

$$C_v\frac{\partial T}{\partial \tau} - H = \nabla_\chi \nabla T, \tag{4}$$

where Ψ is the electrostatic potential, j is the current density, q is the elementary charge, C_v is the specific heat, χ is the thermal conductivity coefficient, T is the temperature, G is the generation rate, and R is the recombination rate. The indices n and p denote electron and hole, respectively.

In spite of the fact that the above equations are generally known, their solution represents a serious mathematical and numerical problems. The reason for the difficulty is the nonlinearity of these equations where carrier densities, ionized dopant densities as well as generation-recombination (g-r) factors are all complex functions of the electrostatic potential Ψ and the quasi-Fermi levels $\Phi_{n,p}$. A number of articles have reported methods of solution of this set of equations, starting from the work of Gummel [14] and de Mari [15], and ending with those adopted in commercial software packages [16,17]. Independently, Jóźwikowski developed a set of numerical algorithms to solve the set of Eqs. (1)–(4). This method has been used for modelling many optoelectronic device structures [18–22]. In the calculations presented in this article a new factor have been included, namely the presence of dislocations.

The numerical method applied in this study employs Newton's algorithm to obtain a steady-state solution to the set of transport equations, using an initial distribution of the electric potential in thermodynamic equilibrium obtained from the condition of electrical neutrality. An iterative approach is then used to solve the Poisson's equation to obtain the electrical potential under equilibrium conditions, which then gives the first trial function in the iterative procedure that leads to the solution of the set of transport Eqs. (1–4) under nonequilibrium conditions. The quasi-Fermi levels used in the first trial function are taken as equal and constant with a value given by the Fermi level in thermal equilibrium.

The difference, G-R is the net generation of electron-hole pairs, and depends on all generation-recombination mechanisms. In this work G-R is defined by

$$\left[G_{ee}\frac{n}{n_0}\left(1-\frac{np}{n_0p_0}\right) + G_{hh}\frac{p}{p_0}\left(1-\frac{np}{n_0p_0}\right) + G_{rad}(n_0p_0 - np) + (n_0 - n)\frac{1}{\tau_e^{SR}}\right]\left(1-\frac{r_0^2}{r_z^2}\right)^{-1}\left(1-\frac{S}{M}\right)^{-1}. \tag{5}$$

Particular terms in quadratic bracket mean speed of generation caused by Auger 1, Auger 7, radiative and SRH mechanisms. The terms outside of quadratic bracket include the effects of dislocation density on thermal generation rate. The parameter r_z is related to a dislocation density, which varies across the device, r_0 is the effective radius of a dislocation core, S refers to the effect of SHR recombination due to the dislocations, and M is the geometric factor. The above expression are derived in the Appendix.

Current density is usually expressed by diffusion and drift contributions described below

$$\vec{j}_p = -qD_p\nabla p - q\mu_p p\nabla\Psi, \tag{6}$$

$$\vec{j}_n = qD_n\nabla n - q\mu_e n\nabla\Psi. \tag{7}$$

However, for structures with large nonuniformities and degenerate regions, these current densities are better expressed as the functions of quasi-Fermi levels

$$\vec{j}_n = q\mu_e n \nabla \Psi_n, \tag{8}$$

$$\vec{j}_n = q\mu_p p \nabla \Psi_p, \tag{9}$$

where μ denotes mobility and D the diffusion constant.

In order to solve the set of transport Eqs. (1)–(4) with relations (8) and (9) using Newton's method, it is necessary to first linearise the equations and then employ an iteration algorithm that allows calculation of small increments of Ψ, Φ_n, Φ_p, and T

$$\Psi = \Psi^0 + \delta\Psi,$$

$$\Phi_n = \Phi_n^0 + \delta\Phi_n,$$

$$\Phi_p = \Phi_p^0 + \delta\Phi_p,$$

$$T = T^0 + \delta T.$$

The remaining physical parameters in Eqs. (1)–(4) can be similarly expressed, for example:

$$n = n(\Psi, \Phi_n) = n^0 + \frac{\partial n}{\partial \Psi}\delta\Psi + \frac{\partial n}{\partial \Phi_n}\delta\Phi_n + \frac{\partial n}{\partial T}\delta T, \tag{10}$$

$$p = p(\Psi, \Phi_p) = p^0 + \frac{\partial p}{\partial \Psi}\delta\Psi + \frac{\partial p}{\partial \Phi_p}\delta\Phi_p + \frac{\partial p}{\partial T}\delta T, \tag{11}$$

$$G - R = G^0 - R^0 + \delta(G - R), \tag{12}$$

where

$$\delta(G-R) = \frac{\delta(G-R)}{\partial n}\left(\frac{\partial n}{\partial \Psi}\delta\Psi + \frac{\partial n}{\partial \Phi_n}\delta\Phi_n + \frac{\partial n}{\partial T}\delta T\right) + \frac{\delta(G-R)}{\partial p}\left(\frac{\partial p}{\partial \Psi}\delta\Psi + \frac{\partial p}{\partial \Phi_p}\delta\Phi_p + \frac{\partial p}{\partial T}\delta T\right). \tag{13}$$

The set of Eqs. (1)–(4) can then be transformed into a set of algebraic equations and their solution allows iterative calculation of corrections to electrical potential, quasi-Fermi levels, and temperature, and consequently to other physical parameters.

3. Modelling and experimental characteristics of high temperature HgCdTe heterostructure photodiodes

Let us consider p$^+$-p-n HgCdTe photodiode structure fabricated using MOCVD technique [23]. Simplified geometry of the device structure, composition and doping concentrations are shown in Fig. 1. The junction area is 0.16 mm^2. The doping concentration in the 3.5-μm thick n-type region is 2×10^{17} cm^{-3} and mole fraction x = 0.333. 5-μm thick p-type epilayer with composition x = 0.27 and doping density of ~10^{16} cm^{-3} is covered by 0.5-μm thick p$^+$-type cap layer with x = 0.321 and acceptor concentration 2×10^{17} cm^{-3}. p$^+$-type cap layer eliminates degenerated influence of electrical top contact on photodiode resistance. Abrupt changes of doping and mole fraction are assumed in the model. The line d indicates direction of calculated spatial distributions of different parameters presented in next figures.

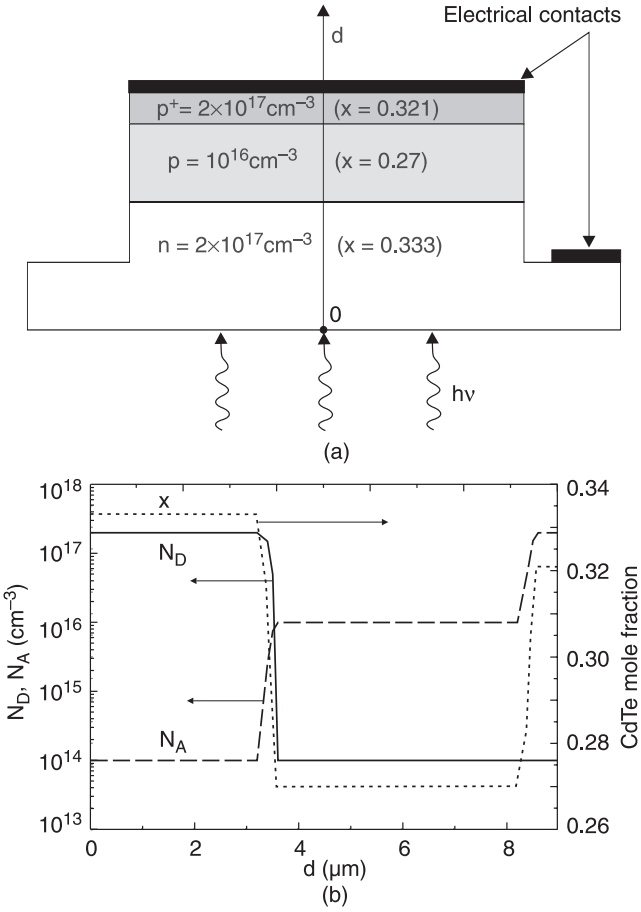

Fig. 1. The cross-section of the investigated HgCdTe photodiode structure (a) and the doping and mole-fraction profiles (b). The line d indicates direction of calculated spatial distributions of different parameters presented in the next figures.

Figure 2 presents the spatial distribution of the electron and hole concentrations together with distribution of dislocation density at 80 mV reserve bias in temperature 240 K. Both electrons and holes in the p-n and p-p$^+$ junctions (also called l-h junction) are extracted by the electrical field caused by the reverse bias, U = 80 mV.

As expected, in the regions with non-uniform distributions of mole-fraction and impurity concentration, strong electric fields are localized. In addition, the graded-gap regions contain considerable misfit dislocation density. It can be shown that the misfit dislocation density can be determined by the following relation [2]

$$N_{DYS}^{INT} = 5\times10^4\,\nabla x, \tag{14}$$

where ∇x is the composition gradient (in cm^{-1}). The parameter N_{DYS}^{INT} can achieve a value as large as 10^9 cm^{-2}.

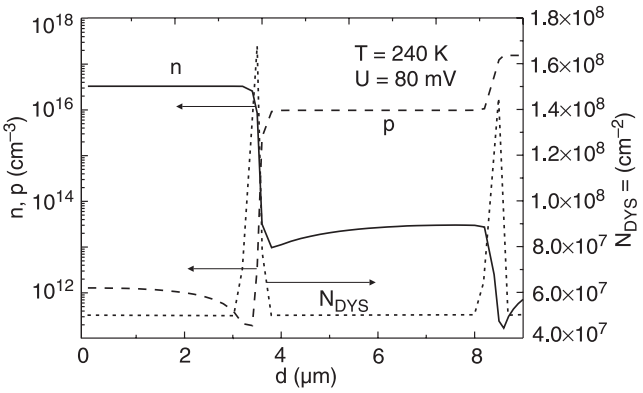

Fig. 2. The spatial distribution of the electron and hole concentrations and the dislocation density in HgCdTe reserve biased (U = 80 mV) heterostructure in temperature 240 K.

In general, the density of dislocation is a sum of contribution from bulk, N_{DYS}^{BULK}, and interface regions N_{DYS}^{INT}.

$$N_{DYS} = N_{DYS}^{BULK} + N_{DYS}^{INT} = N_{DYS}^{BULK} + 5\times10^{4}\,\nabla x. \quad (15)$$

The details of implementation of dislocations into the theoretical model are presented in the Appendix.

The assumed composition and doping concentration profiles permit us to calculate the spatial distribution of band structure of a device and electric field across the device. Figure 3 presents the spatial distribution of the bandgap structure and the electric field along the line d as shown in Fig. 1(a). As expected, the electric field is associated with p-n and p-p$^+$ junctions.

Figures 4 and 5 present destructive influence of electric field on effective speed of carrier recombination in a dislocation region. Reverse bias polarization increases an electric field, especially in the regions of built-in electric fields thereby increasing generation-recombination acts connected with dislocations. This effect is essential in fabricated heterostructures, where the depletion regions of junctions are localized in the regions with extended density of misfit dislocation.

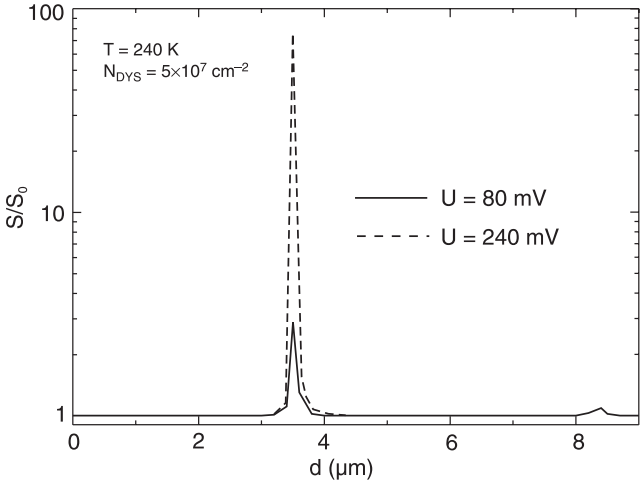

Fig. 4. Influence of reverse bias voltage (U = 80 and 240 mV) on the value of the parameter S which state speed of recombination in dislocation region.

Figure 5 shows the dependence of dynamic resistance versus bias voltage for HgCdTe heterostructure photodiode. Calculations are provided for three different values of dislocation densities in p-type base region of a photodiode. It can be noticed, that in the graded gap regions the dislocation densities are larger than in n-type base region of a photodiode (see Fig. 2). Good agreement of theoretical calculations with experimental results (black points) has been achieved for the dislocation density of 5×10^7 cm^{-3}. However, the theoretical predictions are about two times lower that experimental data for reverse bias above 100 mV. It can be supposed that it is a result of simplified assumption of hyperbolic barrier for electrons transmitted from trap level in the region of dislocation to con-

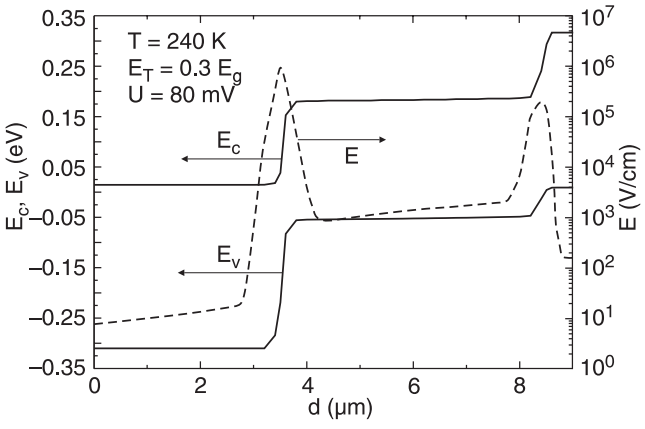

Fig. 3. The bandgap structure of the reverse biased (U = 80 mV) p$^+$-p-n HgCdTe heterostructure at temperature 240 K. Also the spatial distribution of the electric field across the line d [see Fig. 1(a)] is shown (dashed line).

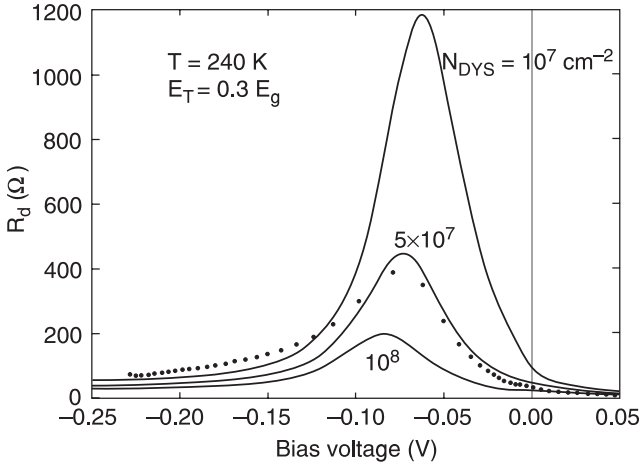

Fig. 5. Dynamic resistance versus bias voltage for three different values of dislocation densities in p-type base region of HgCdTe heterostructure. Experimental results are shown by black points.

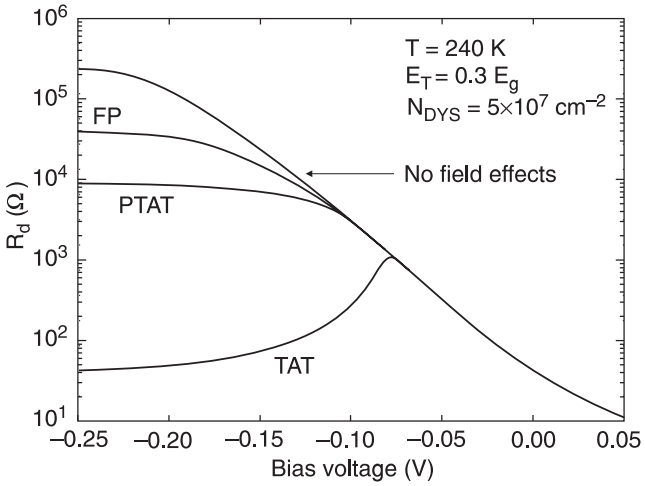

Fig. 6. Influence of Frenkl-Poole effect (FP), tunnelling from trap level with phonon contribution (PTAP) and direct tunnelling from trap level (TAT) on dynamic resistance of HgCdTe photodiode operated at 240 K. The curve marks "No field effect" presents situation when three mentioned mechanisms are not taken into account.

duction band. Assumption of simplifying hyperbolic barrier can cause a systematic error of increasing twice as large of tunnelling current in comparison with a real value.

Figure 6 shows influence of particular mechanisms, enlarged emission coefficient of electrons and holes from a trap level in the region of dislocation, on dynamic resistance versus bias voltage. It results from this figure that the most effective current transport mechanism is TAT, which is predominant for bias voltage above 70 mV. Below this value, the resistance is characterized by a diffusion current.

It is well known that in HgCdTe ternary alloys at room temperature, the Auger mechanism is decisive. Contribution of SRH processes is appreciable barely at considerable reverse bias, when the electric field in depletion region of junction essential increases.

Figure 7 presents exclusion and extraction of carriers as a result of considerable electric field of applied external bias voltage. In general, exclusion and extraction effects decrease thermal Auger generation and overlap on destructive effects connected with activation of SRH centres by an electric field.

Next figure (Fig. 8) shows the spatial distribution of the electric field across HgCdTe heterostructure operated at a room temperature. Similarly as for photodiode operated at 240 K, the electric field has extreme value in the region of p-n junction. Destructive effect of an electric field on minority carrier lifetime and relative coefficient of recombination rate in a region of dislocation is presented in Fig. 9. It can be shown, that the carrier lifetime in depletion junction region can be decreased more than one order of magnitude in comparison with carrier lifetime in a neutral region of a device (outside of a depletion region). This observation is confirmed by Fig. 10, which shows distribution of thermal generation rate across a reverse biased device (U = 250 mV). It is clearly shown that the highest contributions to the thermal generation give two regions of heterojunctions, what has decisive influence on dynamic device resistance.

Figure 11 confirms, that assuming dislocation density on the level of 5×10^7 cm^2 gives the best fitting between experimental data and theory. The same situation has been previously described for devices operated at 240 K (see Fig. 5). It appears that influence of reverse bias on generation-recombination process is not large in reverse bias region below 200 mV. The diffusion current is decisive with contribution of Auger process in a neutral region of a device. It is clearly shown in Fig. 12, where contribution of different mechnisms enlarging emission rate with trap levels is presented. Similarly as for the device operated at 240 K, the most effective current transport mechanism is TAT. However in this case, the TAT is predominant for higher bias voltage – above 200 mV. It is connected with

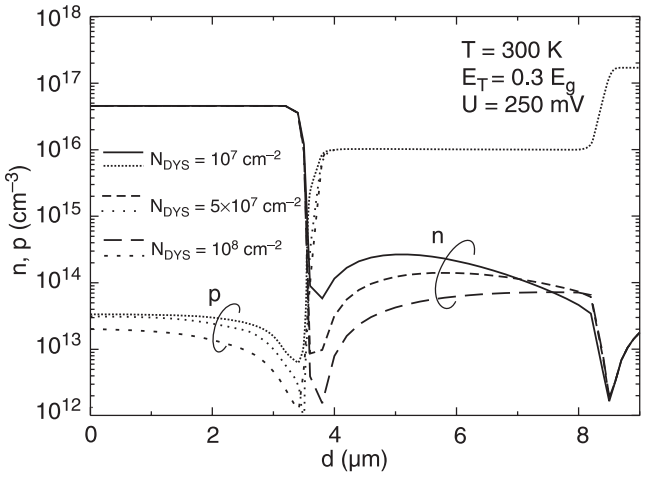

Fig. 7. The spatial distribution of electron and hole concentrations in reverse biased (U = 250 mV) HgCdTe photodiode at temperature 300 K for different dislocation densities.

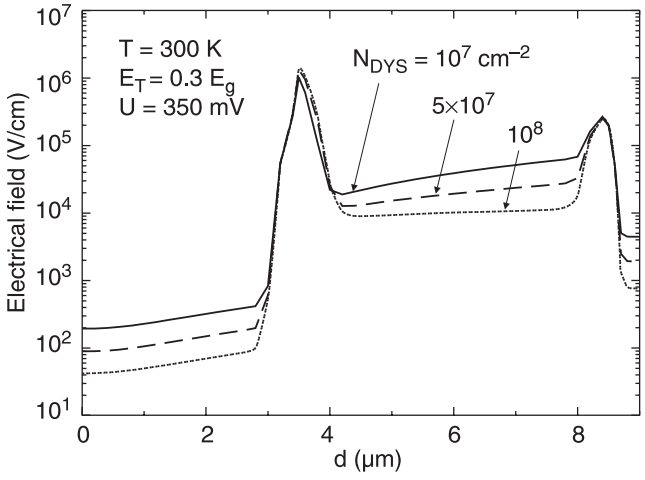

Fig. 8. The spatial distribution of electric field in reverse biased (U = 350 mV) HgCdTe photodiode at room temperature. Calculations are carried out for three levels of dislocation density.

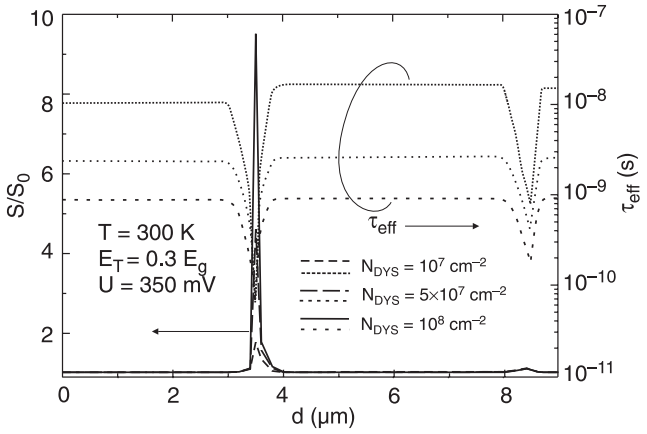

Fig. 9. The spatial distribution of the electric field, minority carrier lifetime and relative coefficient of recombination rate in region of dislocation. Calculations are carried out for three levels of dislocation density. The room temperature HgCdTe heterostructure is reverse biased (U = 350 mV).

considerable greater contribution of the Auger process at a room temperature.

From theoretical simulation of influence of activation energy of the trap level on dynamic photodiode resistance results that the best agreement with experimental data has been achieved assuming that the traps are localized $0.3E_g$ above the top of a valence band. Most likely, however, the localization of a trap level depends on x-composition and temperature in more complicated way.

Figures 13 and 14 present influence of ionization energy of traps localized in dislocation line on dynamic resistance of HgCdTe heterostructure when SRH processes determine the recombination rate. It is connected with decisive influence of TAT mechanism, which exponentially depends on ionization energy of a trap level.

Using two simple models treated ionized atoms in dislocation line as interacted electrostatic point charges or interacted electric dipoles, a number of trapped electrons in

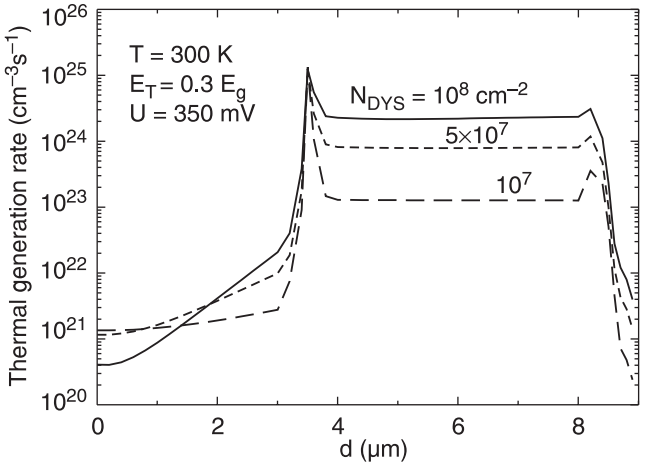

Fig. 10. The spatial distribution of thermal generation rate in room temperature reverse biased (U = 350 mV) HgCdTe heterostructure. Calculations are carried out for three levels of dislocation density.

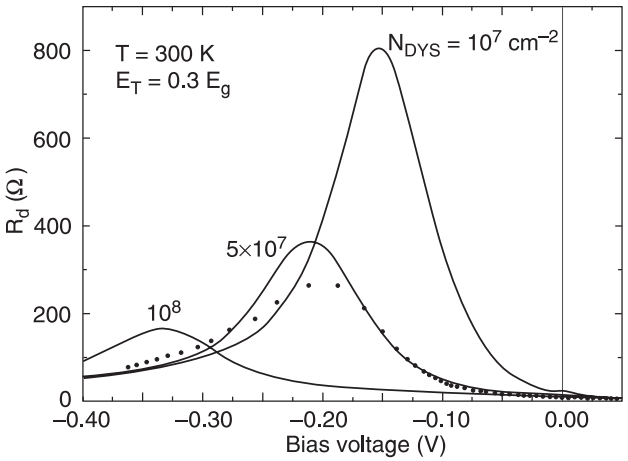

Fig. 11. The dependence of dynamic resitance of room temperature HgCdTe photodiode on bias voltage for three choosen dislocation densities. The best agreement with experimental results (black points) has been achieved for dislocation density of 5×10^7 cm^2.

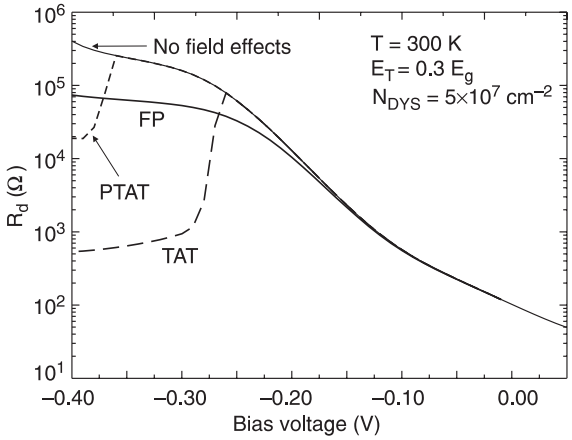

Fig. 12. Influence of Frenkl-Poole effect (FP), tunneling from trap level with phonon contribution (PTAP) and direct tunneling from trap level (TAT) on dynamic resistance of HgCdTe photodiode operated at 300 K. The curve marks "No field effect" presents situation when three mentioned mechanisms are not taken into account.

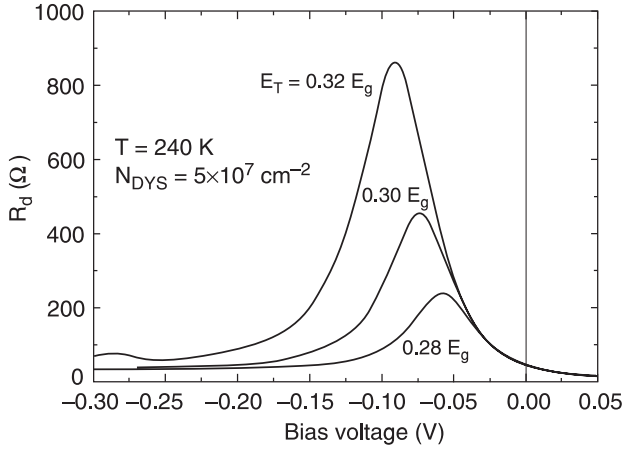

Fig. 13. Dynamic resistance versus bias voltage for three different values of ionization trap energy of dislocations. Calculations are carried out for HgCdTe heterostructure operated at 240 K with dislocation density 5×10^7 cm^2.

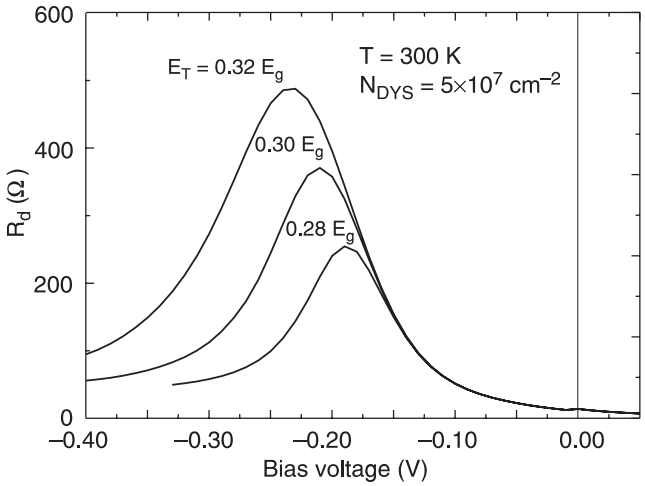

Fig. 14. Dynamic resistance versus bias voltage for three different values of ionization trap energy of dislocations. Calculations are carried out for HgCdTe heterostructure operated at 300 K with dislocation density 5×10^7 cm^2.

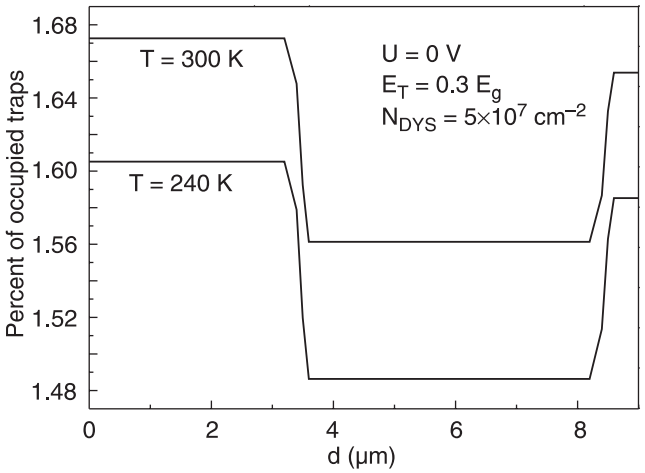

Fig. 15. Percent of occupied traps (ionized metal atoms) along dislocation line *d* (see Fig. 1).

dislocation line have been calculated. Figure 15 shows percent of occupied traps; it means percent of ionized break metal bonds intercepted electrons. In spite of that the number of ionized atoms is about 1.5% for both temperatures (240 and 300 K), however, local electron density on trap levels is extremely large due to comparable size of a region along the dislocation line and the lattice constant.

4. Conclusions

The experimental data of current-voltage characteristics of high temperature MOCVD HgCdTe heterostructure photodiodes operated in the 3–5.5-μm spectral range indicate on significant contributions from tunnelling effects, which dominate the leakage current mechanism for reverse bias greater than a few tens of milivolts. Standard theoretical model does not explain experimental data. To obtain better insight in current-voltage characteristics of real MOCVD HgCdTe heterostructure devices, a two-dimensional model has been developed to investigate the built-in electrical fields on I-V characteristics. It is shown that the presence of regions with high-density misfit dislocations enhances the efficiency of Shockley-Read-Hall generation-recombination processes. In addition to diffusion, generation-recombination and trap assisted tunnelling mechanisms, the Poole-Frankel and phonon-trap assisted tunnelling effects in calculations of dynamic resistance of the junctions have been taken into account. Including of these effects crosses the advantages of non-equilibrium devices out.

It is shown that the most effective current transport mechanism in high temperature HgCdTe heterostructures is trap-assistant tunnelling. In the photodiodes operated at 240 K, this mechanism is predominant at bias voltage that not exceeded 0.1 V. The best fit of experimental data with theoretical predictions for zero bias dynamic resistance versus temperature has been obtained for dislocation density in the bulk of HgCdTe layer equal to 5×10^7 cm^{-2}.

A certain divergence between experimental data and theoretical predictions can result with assumption that that traps are localized $0.3E_g$ above the top of valence band. More physically is assuming Gauss distribution of trap states around average trap energy equal to $0.3E_g$. Such attempt will be taken soon.

Appendix

Fenomenological model of dislocations as areas with excess recombination velocity

Several theoretical models for recombination in the regions surrounding dislocations have been reported [24,25]. In our model the dislocations are considered as cylindrical areas with the radius r_0, the excess surface recombination velocity S, and the average distance between dislocations $2r_z$ (see Fig. A1). Ionised atoms at the dislocation core play the role of Shockley-Read-Hall (SRH) recombination centres and have strong effect on a value of the phenomenological parameter S. The effective lifetime of excess carriers being the function of S allows calculation of the net thermal generation (G–R). The parameters r_0, r_z and S can be estimated from etch pit density and lifetime experiments as reported by Yamamoto *et al*. [2] and Shin *et al*. [3].

The thermal generation in dislocation region can be treated as a bulk process characterized by the bulk recombination rate R (see Fig. A1). Also alternative phenomenological model can be used in which the process on cylindrical surface is described by the surface recombination rate S. Both models are equivalent if simple relation

$$Gh\pi r_0^2 = 2\pi r_0 hS, \tag{A1}$$

is fulfilled. Then

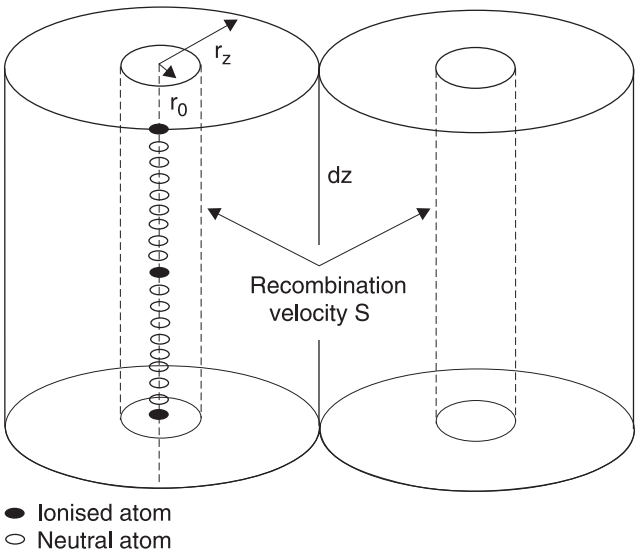

Fig. A1. Dislocations represented as cylindrical areas with radius r_0 and excess surface recombination velocity S. The average distance between dislocations is $2r_z$.

$$G = \frac{2S}{r_0}. \tag{A2}$$

In Ref. 26, the effective carrier lifetime τ_{eff}, in dependence on r_0, r_z and S is given by

$$\tau_{eff} = \tau\left(1 - \frac{r_0^2}{r_z^2}\right)\left(1 - \frac{S}{M}\right), \tag{A3}$$

where

$$M = \frac{r_z^2/r_0 - r_0}{2\tau} + S\left\{1 + 0.25\frac{r_0^2}{D\tau} + \frac{r_z^2}{2D\tau}\left[\gamma + \ln\left(\frac{r_0}{2\sqrt{D\tau}}\right)\right]\right\}. \tag{A4}$$

D is the bipolar diffusion coefficient and τ is given by

$$\frac{1}{\tau} = \frac{\tau_p p\mu_p + \tau_n n\mu_n}{\tau_n\tau_p(p\mu_p + n\mu_n)}, \tag{A5}$$

where n and p are the electron and hole carrier concentrations, respectively, whereas τ_n and τ_p are the electron and hole carrier lifetimes in the region of dislocation core between the radii r_0 and r_z. These carrier lifetimes are determined by band-to-band recombination mechanisms (Auger 1, Auger 7, and radiative recombination) and SRH recombination. It is assumed that in the region of a dislocation core, the main generation-recombination mechanism is SRH process connected with the trap levels created by broken bonds of cadmium and mercury. The electric field enhances generation-recombination process in the dislocation core and through this effect influences the value of the parameter S. So, to ascertain influence of electric field on the parameter S, we can study its dependence on the bulk recombination R [see Eq. (A2)].

For simplicity we assume that the electrons in a conduction band are captured by the traps localized on a dislocation line with the rate R_c^n, which can be expressed by

$$R_c^n = c_n n[N_{DYS} - N_t^-], \tag{A6}$$

where N_{DYS} is the number of trap states in a single dislocation and N_t^- is the number of the ionized traps.

Emission rate with traps is proportional to N_t^-, namely $R_e^n = e_n N_t^-$. So, with equilibrium condition results

$$e_n = c_n n_0 \frac{N_{DYS} - N_t^-}{N_t^-}. \tag{A7}$$

Therefore, the resultant trap rate for an electron is equal to

$$R_n = c_n(n - n_0)[N_{DYS} - N_t^-]. \tag{A8}$$

Analogical considerations for holes captured by traps give the following equations:

- for hole emission coefficient

$$e_p = c_p p_0 \frac{N_t^-}{N_{DYS} - N_t^-}, \tag{A9}$$

- for hole trapping rate

$$R_p = c_p(p - p_0)N_t^-. \tag{A10}$$

In steady state condition $R_n = R_p = R$, and then

$$R = \frac{c_n c_p(n - n_0)(p - p_0)}{c_p(p - p_0) + c_n(n - n_0)} N_D. \tag{A11}$$

Capture coefficients of the electrons and holes, c_n and c_p, depend on ionization energy of a trap level. Similarly as for trap levels connected with point defects, the electric field decreases ionization energy of trap levels connected with dislocations. Three mechanisms considered for point defects; FP, TAT, and PTAT, seem to be the main mechanisms which decrease the ionization energy of dislocation levels.

Figure A2 shows three kinds of electric-field-assisted emissions from a Coulombic well. Arrows indicate the possible mechanisms of electron and hole emissions: Frenkel-Poole emission (FP), pure tunnelling from trap level into conduction or valence bands (TAT), and phonon assisted tunnelling (PTAT).

The parameters δ_n and δ_p determine relative changes of electron and hole emission coefficients with trap levels, and they are enhanced by electric field of FP, TAT and PTAT mechanisms. They are expressed by equations

$$\delta(E) = \frac{(e_p)_{TOT}\, e_p^0}{e_p^0}, \tag{A12}$$

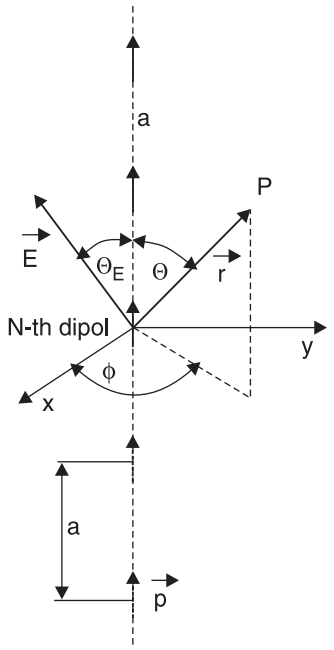

Fig. A2. Atoms along the dislocation line together with neutralizing positive charges make the neutral electrical complexes having significant dipole moments. Interactions between complexes have dipole character. External electric field modified the electric potential around the dislocation line decreasing ionization energy of electron trap in certain directions.

$$(e_n)_{TOT} = (e_n)_{FP} + (e_n)_{TU} + (e_n)_{TAT}, \quad \text{(A13)}$$

and

$$(e_p)_{TOT} = (e_p)_{FP} + (e_p)_{TU} + (e_p)_{TAT}. \quad \text{(A14)}$$

These relations are taken from Ref. 25 [Eqs. (15), (18) and (19) in this paper]; however in this case instead of spherical Coulombic an additional potential of ionized atoms located along the dislocation line should be included, what is shown below. Instead the emission coefficients in the case of absence of electrical field are given by

$$e_n^0 = c_n^0 n_0 \frac{N_{DYS} - N_t^-}{N_t^-}, \quad \text{(A15)}$$

$$e_p^0 = c_p^0 p_0 \frac{N_t^-}{N_{DYS} - N_t^-}, \quad \text{(A16)}$$

where

$$c_p^0 = \sigma_p \langle v_{thp} \rangle \quad \text{(A17)}$$

The thermal coefficients

$$\langle v_{the} \rangle = \left(8k_B T / \pi m_n^*\right)^{1/2}, \quad \langle v_{thp} \rangle = \left(8k_B T / \pi m_p^*\right)^{1/2}. \quad \text{(A18)}$$

The electron and hole capture cross sections, σ_n and σ_p, have been taken as equal to the capture cross sections of point defect trap levels. According to Ref. 4, these values are equal to $\sigma_n = 1.4\times10^{-16}$ cm^2 and $\sigma_p = 1.4\times10^{-16}$ cm^2 for electrons and holes, respectively.

The electric field influences the value of the parameter S owing to a change of effective ionization energy of trap states in a dislocation region. If S_0 means the S-value in absence of electric field, then the surface recombination rate in the electrical field E is equal to

$$S = S_0 \frac{c_p^0(p - p_0) + c_n^0(n - n_0)}{\frac{1}{\delta_n(E)} c_p^0(p - p_0) + \frac{1}{\delta_p(E)} c_n^0(n - n_0)} \quad \text{(A19)}$$

It appears that good potential approximation for point defects is Coulombic spherical potential of point defect [27,28].

In the elaborated model we assumed that if the trap level connected with metal atoms (Hg or Cd) composed saturated bonds in dislocation region is filled by electron, then the atom will be ionized negatively. Ion charge will be neutralized by positive charge (holes or ionized impurities). In such a way, the ionized atom together with neutralizing

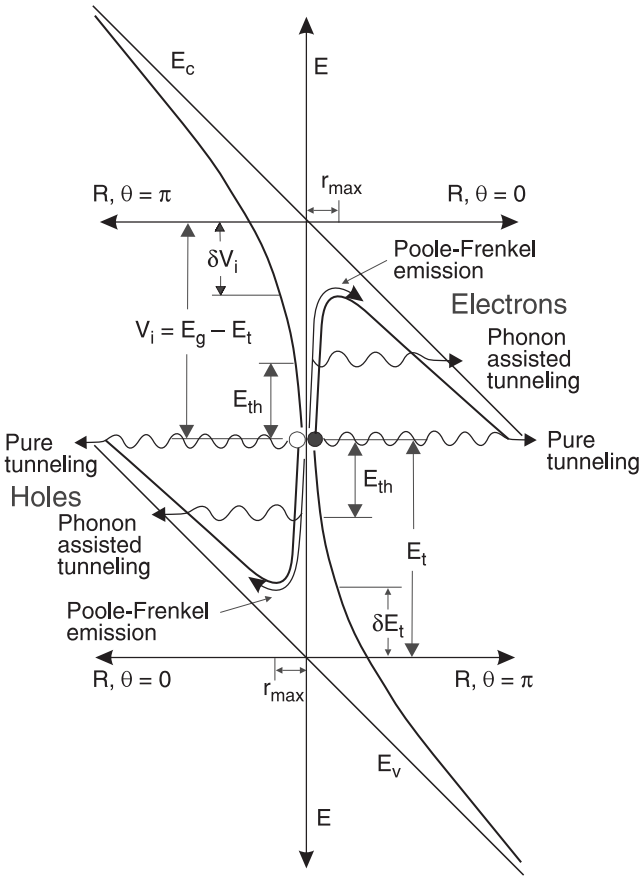

Fig. A3. Three mechanisms increasing emission rate from trap level caused by built-in electric field: Poole-Frenkel emission, pure tunnelling from trap level into conduction or valence bands, and phonon assisted tunnelling. Taking into account these mechanisms the S-parameter is modified.

positive charges make a neutral electrical complex having significant dipole moment. This complex should be interacted as electrical dipole. Ionization energy of a trap level should correspond to the potential energy of a dipole. Hence, the following relation has been assumed [29]

$$E_T = \frac{e^3}{4\pi\varepsilon_r\varepsilon_0 p}, \tag{A20}$$

where p is the complex dipole moment, e is the electron charge, ε_r is the relative dielectric constant, and ε_0 is the vacuum dielectric constant.

It results from the above considerations that the complexes interact through interaction of dipole moments causing their ordering along dislocation line (see Fig. A3). In this way it is possible to found a number of ionized atoms localized along the dislocation line. In this way the ionization energy E_T, is only one fitting parameter, which determines the dipole moment of a single complex.

$$F = -\frac{e^6}{32(\pi 2_r\varepsilon_0 l)^3 E_T^2} N_t^4 - k_B T N_T \times\left[\ln 2 + 1 + \ln\left(\frac{\pi^2 E_T}{e^3 c}\sqrt{\frac{32}{3}(\varepsilon_r\varepsilon_0)^3 k_B T l^5}\right) - \frac{7}{2}\ln N_t\right], \tag{A21}$$

where c is the lattice constant and l is the length of a dislocation line (thread).

A number of complexes (ionized traps) can be calculated with a condition for minimum of free energy

$$\frac{\partial F}{\partial N_T} = 0. \tag{A22}$$

Now, we consider the influence of electric field on energy of electrons localized around a thread of dislocation. It is easily shows that resultant potential of all complexes in the point P is equal to

$$\varphi_n \approx \frac{p}{4\pi\xi_\rho\xi_0}\left\{\frac{\cos\theta}{r^2} + \frac{1}{(a^2 + 2ar\cos\theta + r^2)^{1/2}} - \frac{1}{\left[(n-1)^2 a^2 + 2(n-1)ar\cos\theta + r^2\right]^{1/2}} + \frac{1}{\left[(N_T - n)^2 a^2 + 2(N_T - n)ar\cos\theta + r^2\right]^{1/2}} - \frac{1}{(a^2 - 2ar\cos\theta + r^2)^{1/2}}\right\}. \tag{A23}$$

The most profitable energetic situation (minimum) takes place when interacted complexes are uniformly arranged along a dislocation line. Non-uniformity can be also included assuming that additional energy originates from dipole interaction between the complexes. Using procedure previously proposed by Read [30] for ionized traps treated as point defects, the minimum of free energy can be calculated assuming that dipoles possess the average dipole moment p. It can be shown that the free energy can be given by

To calculate the average value of potential for points localized at the distance $r\sin\theta$ from thread dislocation, averaging the potential φ_n with omitting extreme points is necessary

$$\overline{U} = \frac{1}{N_T}\sum_{n=2}^{N_T-1}\varphi_n. \tag{A24}$$

After approximation of the sums by integrals, we can obtain

$$\overline{\varphi}(r,\theta) = \frac{p}{4\pi\xi_r\xi_0}\left\{\frac{\cos\theta}{r} + \frac{N_t}{l}\left[\frac{1}{\left(\frac{l^2}{N_T^2} + \frac{2lr\cos\theta}{N_T} + r^2\right)^{1/2}} - \frac{1}{\left(\frac{l^2}{N_T^2} - \frac{2lr\cos\theta}{N_T} + r^2\right)^{1/2}}\right] + \frac{N_T}{l^2}\ln\left[\frac{2\left(\sqrt{l^2 + r^2} + l + 2r\cos\theta\right)\left(\sqrt{\frac{2lr}{N_T}\cos\theta + r^2} + \frac{1}{N_T} + r\cos\theta\right)}{\left(2\sqrt{l^2 + r^2 - 2lr\cos\theta} + 2r\cos\theta - l\right)\left(\sqrt{l^2 + r^2 + 2lr\cos\theta} + l + r\cos\theta\right)}\right]\right\}. \tag{A25}$$

Analysing Fig. A2 it can be easily shown, that in the case of the external electrical field E, the electrical potential in the point P equals

$$\varphi(r,\theta,\phi) = \overline{\varphi}(r,\theta) + rE\sin\theta_E\cos\phi + rE\cos\theta_E\cos\theta. \quad \text{(A26)}$$

In this case, the energy making a barrier for emission of electron from dislocation line decreases, instead its value depends on direction in space referred to thread of dislocation and the electric field E. It can be calculated as

$$\delta(r_{\max},\theta,\phi) = -e\varphi(r_{\max},\theta,\phi), \quad \text{(A27)}$$

were $r_{\max}$ is calculated with the condition potential extremum (see e.g. Ref. 28)

$$\frac{\partial\varphi(r,\theta,\phi)}{\partial r}\Big|r = r_{\max} = 0 \quad \text{(A28)}$$

From this condition, the following relation can be achieved

$$\varphi(r,\theta,\phi) = \overline{\varphi}(r,\theta) + \delta_1 Er\sin\theta_E\sin\theta\cos\phi + \delta_2 Er\cos\theta_E\cos\theta, \quad \text{(A29)}$$

where

$$\delta_1 = \begin{cases} 1 & \text{dla } 0<\theta<\frac{\pi}{2},\ 0<\phi<\frac{\pi}{2},\ \frac{\pi}{2}<\theta<\pi,\ \frac{3}{2}\pi<\phi<2\pi, \\ 0 & \end{cases}$$

$$\delta_1 = \begin{cases} 1 & \text{dla } 0<\theta<\frac{\pi}{2}. \\ 0 & \end{cases}$$

The effective ionization energy $E_{T_{eff}}$ can be obtained in the way described by Hartke [28]. In our case it is equal to

$$E_{T_{eff}} = k_B T \ln\left\{\frac{1}{4\pi}\int_0^{2\pi} d\phi \int_0^{\pi} \sin\theta \exp\left[-\frac{E_T - \delta(r_{\max},\theta,\phi)}{kT}\right] d\theta\right\} \quad \text{(A30)}$$

References

1. P. Norton, "HgCdTe infrared detectors", *Opto-Electron. Rev.* **10**, 159–174 (2002).
2. T. Yamamoto, Y. Miyamoto, and K. Tanikawa, "Minority carrier lifetime in the region close to the interface between the anodic oxide CdHgTe", *J. Crystal Growth* **72**, 270–274 (1985).
3. S.H. Shin, J.M. Arias, M. Zandian, J.G. Pasko, and R.E. DeWames, "Effect of the dislocation density on minority-carrier lifetime in molecular beam epitaxial HgCdTe", *Appl. Phys. Lett.* **59**, 2718–2720 (1991).
4. D.L. Polla and C.E. Jones, "Deep level studies of HgCdTe. I: Narrow-band-gap space-charge spectroscopy", *J. Appl. Phys.* **52**, 5118–5131 (1981).
5. D.L. Polla, M.B. Reine, and C.E. Jones, "Deep level studies of HgCdTe. II: Correlation with photodiode performance", *J. Appl. Phys.* **52**, 5132–5138 (1981).
6. D.L. Polla, R.L. Aggarwall, D.A. Nelson, J.F. Shanley, and M.B. Reine, "Hg vacancy related lifetime in HgCdTe by optical modulation spectroscopy", *Appl. Phys. Lett.* **43**, 941–943 (1983).
7. M.E. de Souza, M. Boukerche, and J. P. Faurie, "Minority-carrier lifetime in p-type (111)B HgCdTe grown by molecular-beam epitaxy", *J. Appl. Phys.* **68**, 5195–5199 (1990).
8. R. Fastow and Y. Nemirovsky, "The excess carrier lifetime in vacancy- and impurity-doped HgCdTe", *J. Vac. Sci. Technol.* **A8**, 1245–1250 (1990).
9. M.C. Chen, R.S. List, D. Chandra, M.J. Bevan, L. Colombo, and H.F. Schaake, "Key performance-limiting defects in p-on-n HgCdTe heterojunction infrared photodiodes", *J. Electron. Mater.* **25**, 1375–1382 (1996).
10. S. Barton, P. Capper, C.L. Jones, N. Metcalfe, and D. Dutton, "Determination of Shockley-Read trap parameters in n- and p-type epitaxial $Cd_xHg_{1-x}Te$", *Semicond. Sci. Technol.* **11**, 1163–1167 (1996).
11. A. Rogalski, K. Adamiec, and J. Rutkowski, *Narrow-Gap Semiconductor Photodiodes*, SPIE Press, Bellingham, 2000.
12. W. Van Roosbroeck, "Theory of the electrons and holes in germanium and other semiconductors", *Bell Syst. Tech. J.* **29**, 560–607 (1950).
13. M. Kurata, *Numerical Analysis of Semiconductor Devices*, Lexington Books, DC Heath (1982).
14. H.K. Gummel, "A self-consistent iterative scheme for one-dimensional steady state transistor calculations", *IEEE Trans. Electron Devices* **ED 11**, 455–465 (1964).
15. A. De Mari, "An accurate numerical steady-state one-dimensional solution of the p–n junction", *Solid State Electronics* **11**, 33–58 (1968).
16. Software: *Semicond Devices*, Dawn Technologies, Inc. California.
17. Software: *Apsys*, Crosslight Software, Inc. Ontario, Canada.
18. K. Jóźwikowski, J. Piotrowski, K. Adamiec, and A. Rogalski, "Computer simulation of HgCdTe photovoltaic devices based on complex heterostructures", *Proc. SPIE* **3629**, 74–80 (1999).
19. K. Jóźwikowski, "Computer simulation of non-cooled long wavelength multi-junction (Cd,Hg)Te photodiodes", *Infrared Phys. & Technol.* **41**, 353–359 (2000).
20. K. Jóźwikowski and A. Rogalski, "Effect of dislocations on performance of LWIR HgCdTe photodiodes", *J. Electron. Mater.* **29**, 736–741 (2000).
21. K. Jóźwikowski and A. Rogalski, "Computer modelling of dual-band HgCdTe photovoltaic detectors", *J. Appl. Phys.* **90**, 1286–1291 (2001).
22. K. Jóźwikowski, W. Gawron, J. Piotrowski, and A. Jóźwikowska, "Enhanced numerical modelling of non-cooled long-wavelength multi-junction (Cd,Hg)Te photodiodes", *IEE Proc.-Circuits Devices Syst.* **150**, 65–71 (2003).
23. A. Piotrowski, P. Madejczyk, W. Gawron, K. Kłos, M. Romanis, M. Grudzień, A. Rogalski, and J. Piotrowski, "MOCVD growth of $Hg_{1-x}Cd_xTe$ heterostructures for uncooled infrared photodetectors", *Opto-Electron. Rev.* **12**, 453–458 (2004).
24. S.M. Johnson, D.R. Rhiger, J.P. Rosbeck, J.M. Peterson, S.M. Taylor, and M.E. Boyd, "Effect of dislocations on the

electrical and optical properties of long-wavelength infrared HgCdTe photovoltaic detectors", *J. Vac. Sci. Technol.* **B10**, 1499–1506 (1992).
25. K. Jóźwikowski and A. Rogalski, "Effect of dislocations on performance of LWIR HgCdTe photodiodes", *J. Electron. Mater.* **29**, 736–741 (2000).
26. K. Jóźwikowski and T. Niedziela, "The influence of dislocations on generation-recombination process in narrow-bandgap semiconductor", *Electron Technology* **33**, 518–528 (2000).
27. E. Rosencher, V. Mosser, and G. Vincent, "Transient-current study of field-assisted emission from shallow levels in silicon", *Phys. Rev.* **B29**, 1135–1147 (1984).
28. J.L. Harthe, "The three-dimensional Poole-Frenkel effect", *J. Appl. Phys.* **39**, 4871–4873 (1968).
29. P.A. Martin, B.G. Streetman, and K. Hess, "Electric field enhanced emission from non-Coulombic traps in semiconductors", *J. Appl. Phys.* **52**, 7409–7415 (1981).
30. W.T. Read, "Statistics of the occupation of dislocation acceptor centres", *Phil. Mag.* **45**, 1119–1128 (1954).

